An Inclusive Search for Long-lived Decays with the CMS Detector at the Large Hadron Collider in $\sqrt{s} = 13$ TeV Data

Joshua Robert Hardenbrook

A Dissertation
Presented to the Faculty
of Princeton University
in Candidacy for the Degree
of Doctor of Philosophy

Recommended for Acceptance
by the Department of
Physics
Adviser: Christopher G. Tully

2017

Abstract

A search for long-lived particles decaying to jets is presented, performed on the data collected by CMS at a center-of-mass energy $\sqrt{s} = 13$ TeV in 2015. The data set corresponds to an integrated luminosity of 2.7 fb^{-1}. The analysis exploits a set of trigger algorithms and a customized displaced-jet tagger. The number of tagged displaced-jets is used to characterize a potential signal. The pair production of long-lived particles decaying to two jets or to a b jet and a lepton is excluded for masses lighter than 450–1000 GeV, for lifetimes between 1 mm to 1 m.

Acknowledgements

This is where I acknowledge peeeeeepople

This is the dedication all about how my thesis got turned right upside down

Contents

Chapter 1

Introduction

1.1 The Standard Model

Standard model things [1]

Chapter 2

Experimental Setup

2.1 Founding and History

2.2 Large Hadron Collider

2.3 Other LHC Related Experiments

2.4 Compact Muon Solenoid Experiment

2.4.1 ECAL

2.4.2 HCAL

2.4.3 Tracking

2.4.4 Muon Chambers

2.4.5 Trigger System

Level 1 (L1) Trigger

High Level Trigger (HLT)

Chapter 3

Theory

3.1 Standard Model of Particle Physics

3.1.1 Quantum Field Theory

3.1.2 Gauge Symmetries

3.1.3 The Narrow Width Approximation

3.1.4 Electroweak Symmetry Breaking

3.2 Supersymmetry

3.3 Electroweak Symmetry Breaking

Chapter 4

Strategies for Discovering New Physics at the LHC

Chapter 5

Displaced Jet Analysis

5.1 Introduction

The study of physics beyond the standard model (BSM) is one of the main objectives of the ATLAS and CMS experiments at the CERN LHC. With no signal observed so far, the ATLAS and CMS results put severe bounds on BSM theories.

The majority of these searches focus on prompt particles with lifetimes $c\tau_0 <$ 1mm and contain requirements on the physics objects that reject longer lived particle decays. This leaves open the possibility that light long-lived particles could exist and still remain undetected. In this paper, we present an inclusive search for long-lived particles decaying to various combinations of jets and leptons. The analysis exploits the information originating from the CMS calorimeters to reconstruct jets and measure their energies. The information from reconstructed tracks, in particular the transverse impact parameters, is used to discriminate the displaced-jets signal from the background of ordinary multijet events. The analysis is performed on data collected with the CMS detector at a center-of-mass energy $\sqrt{s} = 13$ TeV in 2015. The data set corresponds to an integrated luminosity of 2.7fb^{-1}. Results for similar

signatures have been reported by ATLAS [2, 3] and CMS [4], using data collected at $\sqrt{s} = 8$ TeV.

5.2 Datasets

5.3 An inclusive displaced-jet tagger

5.4 Event selection

A signal is searched for by applying the selection described in section **??** and counting the number of tagged displaced jets, N_{tags}. In addition to the online and offline requirements described in section 5.5, the analysis signal region requires $N_{\text{tags}} \geq 2$. Efficiencies are reported for all interpreted models as a function of the lifetime with fixed mass (Table 5.1 and 5.2) as well as a function of mass with fixed lifetime (Table 5.3 and 5.4).

The two classes of events: (i) events passing the inclusive trigger algorithm and with $H_{\text{T}} > 650$ GeV; (ii) events passing the exclusive trigger algorithm and with $H_{\text{T}} > 450$ GeV are treated as a single class.

5.5 Datasets and simulated samples

Events are collected from two dedicated online selection algorithms, designed to identify events with displaced jets. The algorithms consider jets clustered from energy deposits in the calorimeters, using the FASTJET [5] implementation of the anti-k_t algorithm [6], with size parameter 0.4. Jets with transverse momentum $p_t < 60$ GeV or $|\eta| > 2.0$ are discarded. An inclusive trigger algorithm accepts events when the scalar sum of the jet p_t's, H_{T}, is greater than 500 GeV and at least two jets with $|\eta| < 2.0$ and at most two prompt tracks are found. Tracks are classified as prompt if

Table 5.1: Signal efficiency for fixed $m_X = m_{\tilde{t}} = 300$ GeV and varied $c\tau_0$ for the Jet-Jet and B-Lepton models. Selection requirements are cumulative from the first to the last row.

Jet-Jet

m_X [GeV]	300	300	300	300
$c\tau_0$ [mm]	1	10	100	1000
≥ 2 tags	2.33 ± 0.15%	39.49 ± 0.63%	54.54 ± 0.74%	14.58 ± 0.38%
Trigger	2.16 ± 0.15%	38.12 ± 0.62%	39.32 ± 0.63%	8.07 ± 0.28%
Event sel.	2.09 ± 0.14%	37.09 ± 0.61%	36.53 ± 0.60%	6.67 ± 0.26%
≥ 3 tags	0.170 ± 0.041%	14.14 ± 0.38%	16.72 ± 0.41%	1.36 ± 0.12%
≥ 4 tags	0.010 ± 0.010%	4.73 ± 0.22%	4.71 ± 0.22%	0.170 ± 0.041%

B-Lepton

$m_{\tilde{t}}$ [GeV]	300	300	300	300
$c\tau_0$ [mm]	1	10	100	1000
≥ 2 tags	0.453 ± 0.023%	15.82 ± 0.13%	31.52 ± 0.19%	8.545 ± 0.098%
Trigger	0.291 ± 0.018%	11.45 ± 0.11%	17.08 ± 0.14%	3.224 ± 0.060%
Event sel.	0.269 ± 0.017%	9.91 ± 0.11%	13.33 ± 0.12%	2.084 ± 0.048%
≥ 3 tags	0.017 ± 0.004%	2.462 ± 0.053%	3.814 ± 0.065%	0.368 ± 0.020%
≥ 4 tags	–	0.297 ± 0.018%	0.480 ± 0.023%	0.0315 ± 0.0060%

their transverse impact parameter relative to the beam line, IP^{2D}, is less than 1mm. Another trigger algorithm is used, which requires $H_T > 350$ GeV and asks that there be two displaced jets each having at least one track with transverse impact parameter $IP^{2D} > 5\sigma_{IP^{2D}}$, where $\sigma_{IP^{2D}}$ is the uncertainty on IP^{2D}. Samples with large H_T are used to study the performance of the online selection algorithms.

Events are selected offline requiring at least two jets with $p_t > 60$ GeV and $|\eta| < 2.0$. As for the online selection, the offline jet reconstruction is performed clustering energy deposits in the calorimeters with the anti-k_t algorithm, with jet size parameter of 0.4. Two classes of events are considered: (i) events passing the inclusive trigger algorithm and with $H_T > 650$ GeV and (ii) events passing the exclusive trigger algorithm and with $H_T > 450$ GeV. The two classes of events sum to 786,002 unique events passing the event selection.

The main source of background events originates from multijet production. The properties of this background process are studied using a simulated multijet sample, generated with PYTHIA 8 [7]. The NNPDF 2.3 [8] parton distribution functions (PDFs) are used to model the parton momentum distribution inside the colliding protons. The event simulation includes the effect of multiple proton-proton collisions in the same bunch crossing and in bunch crossing nearby in time, referred to as pileup. Simulated samples are reweighted to match the pileup profile observed in data.

The analysis is interpreted with a set of benchmark signal models. The **Jet-Jet** model predicts pair-produced long-lived scalar neutral particles X^0 [9], each decaying to two light quarks u,d,s,c, and b with equal probability. The resonance mass m_X and proper lifetime $c\tau_0$ are scanned between 50 and 1500 GeV and between 1 and 2000mm, respectively. The trigger efficiencies for a fixed $m_X = 300$ GeV and $c\tau_0 = 1, 30$, and 1000 mm are 30%, 81%, and 42% respectively. The trigger efficiencies for a fixed $c\tau_0 = 30$ mm and $m_X = 50, 100$, and 1000 GeV are 2%, 14%, and 92% respectively.

The **B-Lepton** model contains pair-produced long-lived top squarks in R-parity violating models of Supersymmetry [10]. Each top squark decays to one b quark and a lepton. The branching fractions of the decay to the three lepton flavors are equal. The resonance mass $m_{\tilde{t}}$ and proper lifetime $c\tau_0$ are scanned between 300 and 1000GeV and between 1 and 1000mm, respectively. The trigger efficiencies for a fixed mass $m_{\tilde{t}} = 300$ GeV and $c\tau_0 = 1, 30$, and 1000 mm are 15%, 41%, and 23% respectively. The trigger efficiencies for $m_{\tilde{t}} = 500, 700$, and 1000 GeV and fixed $c\tau_0 = 30$ mm are 64%, 71%, and 74% respectively.

These models are also investigated with modified branching fractions. The **Light-Light** model is the Jet-Jet model excluding decays to b quarks (equal decays to lighter quarks) and the **B-Mu**, **B-Ele**, and **B-Tau** models are derived from the B-Lepton model with 100% branching fraction to muons, electrons, and taus, respectively. Lep-

tonic tau decays are included in the **B-Tau** interpretation. All signal samples are generated with PYTHIA, with the setup described above for the multijet sample.

5.6 Background prediction

As typical multijets contain only a sub dominant fraction of real displaced tracks, jets with a small multiplicity of tracks represent the dominant background. As the tagging criteria utilize averages of all tracks matched to the jet, the likelihood of tagging a fake decreases exponentially with N_{tracks}.

Figure 5.1 shows the fraction of jets that are tagged as displaced jets in data as a function of the number of tracks associated with the jet N_{tracks}. This function is the misidentification rate of tagging a prompt jet as displaced (up to possible signal contamination) and is interpreted as the probability $p(N_{\text{tracks}})$ of being tagged. This parameterization allows for a representative estimation, event by event, of the probability of tagging multiple fake displaced jets. That is to say, an event with two high track multiplicity jets is much less probable than two single track jets to have 2 fake displaced-jet tags.

To maintain the statistical independence of the events that are used to perform the prediction and the events in the signal region, the probabilities are measured in the full control sample of events with $N_{\text{tags}} \leq 1$, while the final signal region requires $N_{\text{tags}} \geq 2$. Additionally, this limits signal contamination in the probability measurement. The control sample of $N_{\text{tags}} = 1$ includes 1391 events.

The size of the bias introduced by only measuring the misidentification rate in events with $N_{\text{tags}} \leq 1$ is quantifiable. For the nominal tag the size of the effect of removing these events on the predicted number of two tag events is negligible (0.4%) compared to the statistical uncertainty of the prediction.

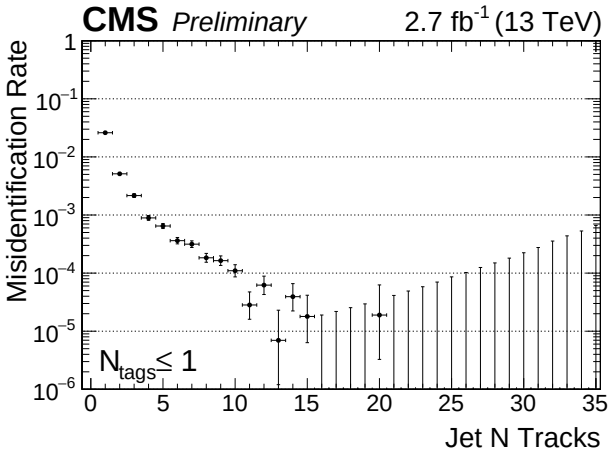

Figure 5.1: The fraction of jets passing the displaced-jet tagging criteria as a function of the number tracks associated with the jet N_{tracks}. The results are from data events with $N_{\text{tags}} \leq 1$ collected with the displaced-jet triggers and passing the offline selection criteria.

The mistagging rate is used to predict the probability for an event to have N_{tags} tagged jets, $P(N_{\text{tags}})$. For instance, for an event m with three jets j_1, j_2, and j_3, there is one configuration with no tags, with a probability:

$$P^m(N_{\text{tags}} = 0) = (1 - p_1)(1 - p_2)(1 - p_3) \ ,$$

where $p_i = p(N_{\text{tracks}}(j_i))$. Similarly, there are three possibilities for this same event to have $N_{\text{tags}} = 1$:

$$P^m(N_{\text{tags}} = 1) = p_1(1 - p_2)(1 - p_3) + (1 - p_1)p_2(1 - p_3) + (1 - p_1)(1 - p_2)p_3 \ .$$

The probability of finding N_{tags} tags in the m event is:

$$P^m(N_{\text{tags}}) = \sum_{\text{jet-configs}} \prod_{i \in \text{tagged}} p_i \prod_{k \in \text{not-tagged}} (1 - p_k) \ . \tag{5.1}$$

Tagged jets enter the product as p_i and non-tagged jets enter as $(1-p_i)$. Equation (5.1) is used to compute the probability of observing N_{tags}, under the assumption that the sample does not contain any signal. The number of events expected for a given value of N_{tags} is then computed as

$$N_{\text{events}}(N_{\text{tags}}) = \sum_m P^m(N_{\text{tags}}) \ , \tag{5.2}$$

where m runs only over events with fewer than two tagged jets. The prediction is then compared to the observed N_{tags} multiplicity in events with two or more tagged jets, to assess the presence of a signal.

We validate this procedure in the absence (background-only test) and presence (signal-injection test) of a signal, using simulated events.

The background-only test is performed predicting the tag multiplicity on the simulated multijet sample, taking as input the misidentification rate distribution. In order to populate the large-N_{tags} region of the distribution, a looser version of the displaced-jet tagger is employed in this test. The full sample of events passing the event selection is divided into multiple independent samples and the background prediction validated. The predicted background of N_{tags} events in simulated multijet events is found to be consistent within statistical uncertainty.

5.6.1 Signal Injection Tests

Injection with QCD

To test the response of the background prediction to the presence of signal contamination in the jet probabilities used for the $P(N_{tags})$ derivation, signal events are 'injected' into QCD Monte Carlo. Approximately 15 million QCD events from /QCD_HT700to1000_TuneCUETP8M1_13TeV-madgraphMLM-pythia8 are used as the background input. The resulting predictions for varied masses, lifetimes, and sizes

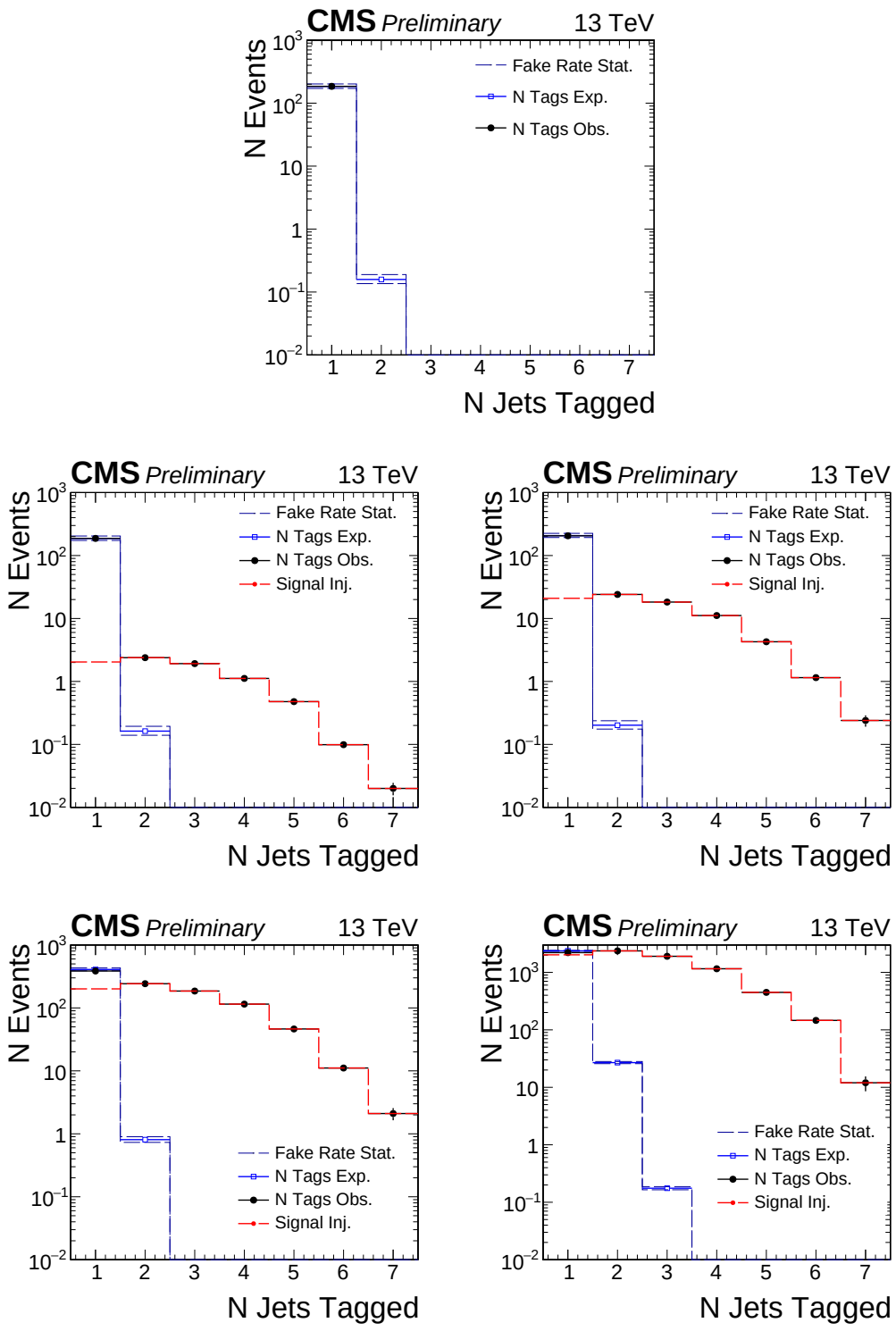

Figure 5.2: Signal Injection tests. The Jet-Jet signal sample used has fixed m_X = 700GeV and $c\tau_0$ = 10 mm. The level of signal contamination is progressively varied between 10, 100, 1000, and 10000 events injected before any selection. The full event selection is applied and the baseline jet tag definition.

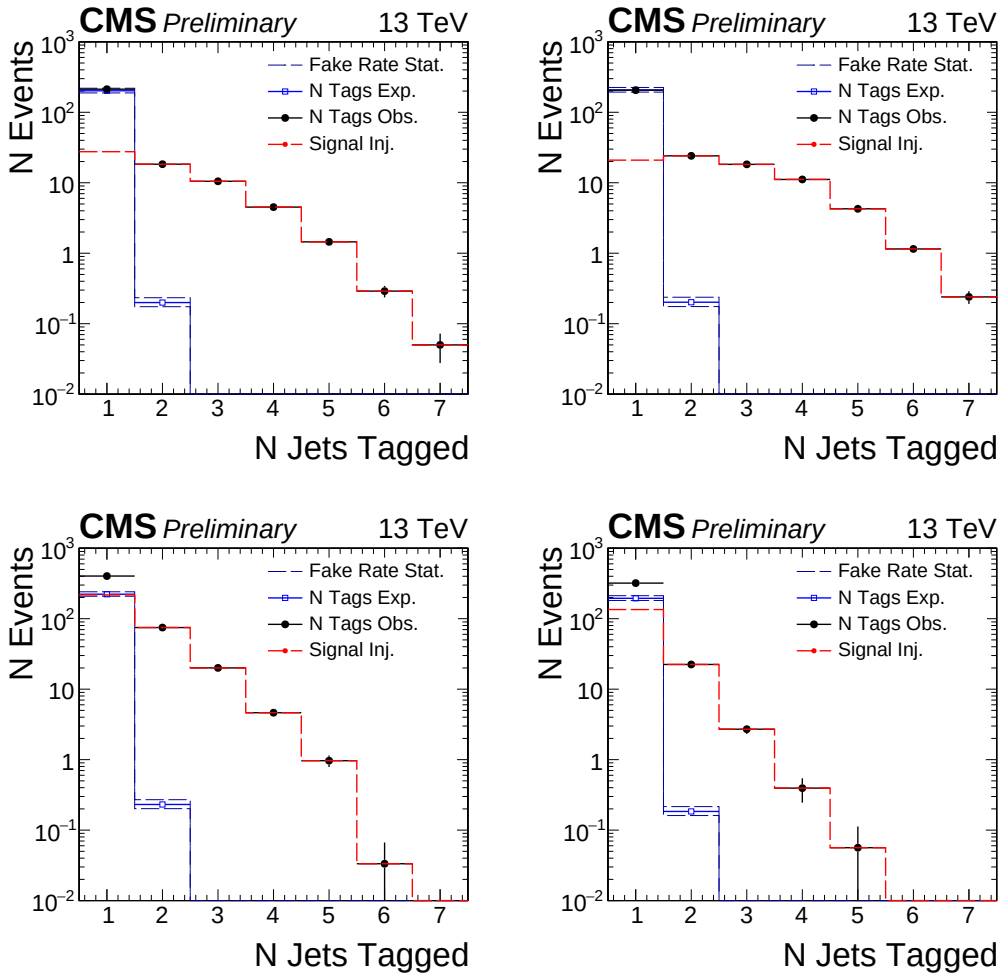

Figure 5.3: Signal Injection. The Jet-Jet signal sample is varied $m_X = 700$ GeV and $c\tau_0 = 1000$ mm (top left) $m_X = 700$GeV and $c\tau_0 = 10$ mm (top right) $m_X = 100$GeV and $c\tau_0 = 1000$ mm (bottom left) $m_X = 100$ GeV and $c\tau_0 = 10$ mm (bottom right). The level of signal contamination is fixed at 100 events for the $m_X = 700$ GeV and 1000 events for $m_X = 100$ GeV. The full event selection is applied and the baseline jet tag definition.

of contamination are shown in Fig. 5.2 and Fig. 5.3. The corresponding predictions, observed number of tags, and the deviation from expectation are summarized in Table 5.5 and Table 5.6. The goal of this exercise is to understand the quantity of signal contamination, as well as lifetime and mass, required to significantly alter the background prediction.

The resulting predictions are also reported normalized such that the total signal + qcd events passing the event selection are equal to the number of events passing the event selection in the analysis in Table 5.7.

The change in the N_{tags}^{obs} distribution to the presence of signal is on the order of the number of events with $N_{tags} > 2$ whereas the integrated shift in $P(N_{tags} \geq 2)$ is on the order of the shift induced in the $p(j)$ distribution. This shift is of the order the signal contamination. We can conclude the analysis will retain relative sensitivity as long as the signal contamination is relatively smaller than the QCD contribution in the fake rate calculation.

In summary, the background prediction is robust to a variety signal masses, lifetimes and sizes of contamination. Robust in the sense that the background is correctly determined within error in the 0 injection case and the bias to the background prediction due to the contamination is small relative to the number of signal events injected.

The following section explores the sensitivity to signal explicitly in a simplified scenario given the assumption that the jet probabilities accurately predict the background in the scenario where there are no signal events present. This assumption is based on on the the closure studies in the previous section and be considered true within some closure systematic.

Explicit Sensitivity in A Simplified Injection Scenario

Consider a sample of N_{QCD} QCD events with a known fraction of jets that are tagged $f(j_i)$ as a function of some jet parameters j_i. For simplicity, assume events have exactly 2 jets. Also assume we have shown that the observation approximately determined $N_{obs}^{2tag} = N_{pred}^{2tag}$ when we interpret $f(j_i)$ as a conditional probability $p(j_i)$ such that:

$$N_{obs}^{2tag} = N_{pred}^{2tag} = \sum_i [p(j_1)p(j_2)]_i = N_{QCD}p^2$$

where we are using a flat probability p such that $p(j_1) = p(j_2) = p = n_{tag}/n_{jets} = n_{fake}/2N_{events}$. Where n_{tag} is the number of jets tagged, which in a QCD sample is exactly n_{fake}. Now, say we perform the signal injection test by injecting N_{sig} events with correspondingly $2N_{sig}$ signal jets. Let ϵ be the efficiency for a signal event to have 1 tag. Accordingly the probability will shift $p(j_i) \to \tilde{p}(j_i)$:

$$\tilde{p} = \frac{n_{fake} + n_{true-tags}}{2N_{QCD} + 2N_{sig}} = \frac{n_{fake} + \epsilon 2N_{sig}}{2N_{QCD} + 2N_{sig}}$$

Taylor expanding in N_{sig} about 0 we obtain:

$$\begin{aligned}\tilde{p} &= \frac{n_{fake}}{2N_{QCD}} - \frac{N_{sig}n_{fake}}{2(N_{QCD})^2} + \epsilon\frac{2N_{sig}N_{QCD}}{2(N_{QCD})^2} \\ &= p - p\frac{N_{sig}}{N_{QCD}} + \frac{N_{sig}\epsilon}{N_{QCD}}\end{aligned}$$

Let $\Delta = N_{sig}/N_{QCD}$

$$\tilde{p} = p(1 - \Delta) + \Delta\epsilon$$

Note that as the signal contamination $\Delta \to 0$, we obtain the correct probability $\tilde{p} = p$. Now we attempt to predict the number of events with 2 tags using $\tilde{p}$ and splitting

the sum over signal and QCD events.

$$\begin{aligned} N_{pred}^{2tag} &= \sum_i \tilde{p}\tilde{p} \\ &= \sum_i (p(1-\Delta)+\Delta\epsilon)^2 \\ &= \sum_i p^2 - p^2(2\Delta) + p^2\Delta^2 + 2p\Delta\epsilon - 2p\Delta^2\epsilon + \Delta^2\epsilon^2 \end{aligned}$$

We now split the events in the sum between QCD and Signal.

$$\begin{aligned} N_{pred}^{2tag} &= \sum_i (QCD) + \sum_i (Signal) \\ \sum_i (QCD) &= N_{QCD}(p^2 - p^2(2\Delta) + p^2\Delta^2 + 2p\Delta\epsilon - 2p\Delta^2\epsilon + \Delta^2\epsilon^2) \\ &= N_{obs}^{QCD} - N_{sig}(p^2\Delta + \Delta\epsilon^2 - 2p^2 + 2p\epsilon - 2p\Delta\epsilon) \end{aligned}$$

where we have used the fact that $\Delta N_{QCD} = N_{sig}$ and $\sum_i p^2 = N_{obs}^{QCD}$:

$$\sum_i (Signal) = N_{sig}(p^2 - p^2(2\Delta) + p^2\Delta^2 + 2p\Delta\epsilon - 2p\Delta^2\epsilon + \Delta^2\epsilon^2)$$

We now evaluate our sensitivity to signal or equivalently the disagreement between observed and prediction by the variable S. Let $N_{obs}^{2tag} = N_{obs}^{sig} + N_{obs}^{QCD}$. The sensitivity S, is a measure of how well we have predicted the background in the presence of signal. When $S = 1$ the prediction is exactly the background and the excess is exactly the number of signal events. When $S = 0$ the probabilities prediction has over estimated the background entirely resulting in no disagreement between observed and predicted

2 tag events.

$$S = \frac{N_{obs}^{2tag} - N_{pred}^{2tag}}{N_{sig}} = 1 - (2p\epsilon + \Delta\epsilon^2) \\ - (p^2 + \Delta^2\epsilon^2 + 2p\Delta\epsilon - 2p^2 - 2p\Delta\epsilon) \\ - (p^2\Delta - 2p^2\Delta - 2p\Delta^2\epsilon) \\ - (p^2\Delta^2)$$

where we have grouped terms by their order in $O(\Delta) + O(p)$. Consider the case when $\epsilon \approx 1$ (this is an approximation for readability as $\epsilon = 1$ would imply no 2 tag events) and for simplicity say $\Delta = p = x$.

$$S = 1 - 3x + 3x^3 - x^4$$

If we plug in the baseline fake rate for x then $S(x = 5 \times 10^{-4}) = 0.999$.

5.7 Systematic uncertainties

5.7.1 Background systematic uncertainties

A background systematic uncertainty is quoted for the data-driven background prediction method. This uncertainty is estimated by repeating the background-prediction procedure on data with a looser version of the displaced-jet tagging algorithm as outlined in section 5.6. The background estimation uncertainty of 7.5% is the required adjustment to the prediction to remove the bias observed in the Gaussian fit. For three or more tags, the systematic uncertainty for the method is kept fixed.

The statistical uncertainty on the measured misidentification rate as a function of N_{tracks} is propagated to the predicted N_{tags} distribution as a systematic uncertainty.

This systematic uncertainty is calculated for each tag multiplicity bin individually. The uncertainty for the 2 tag bin is $-12/+13\%$.

In summary, for the background prediction in the two tag bin, a 7.5% uncertainty is assigned to the background prediction method and $-12/+13\%$ uncertainty is assigned to the statistics of the misidentification rate.

5.7.2 Signal systematic uncertainties

A summary of the systematic uncertainties associated with the signal yields is given in Table 5.8. The uncertainty on the trigger emulation is measured by comparing the predicted efficiency for simulated multijet events and data collected by a loose H_{T} trigger. The observed difference at threshold (5%) is taken as an estimate of the uncertainty in the emulation of the online H_{T} requirement. Similarly, the uncertainty induced by the online versus offline jet acceptance is obtained from the shift in the trigger efficiency when the offline jet p_t requirement is increased from $p_t > 60$ GeV to $p_t > 80$ GeV (5%).

The systematic uncertainty on the luminosity is 2.7% [11].

The uncertainty arising from the PDFs for pair-produced masses in the range of 50–1500GeV is found to be 1–6%. An ensemble of alternative PDF is sampled from the output of the NNPDF fit. Events are reweighted according to the ratio between these alternative PDF sets and the nominal ones. The distribution of the signal prediction for these PDF ensemble is used to quantify the uncertainty.

The systematic uncertainty on the modeling of the jet tagging variables in signal MC samples is estimated from the displaced track modeling in multi-jet events in data and MC. The mismodeling of the measured value of Θ_{2D} and $IP^{\mathrm{2D}}_{\mathrm{sig}}$ for single tracks is propagated to the final tag distribution by varying the individual measured values in MC by the difference in the measured value relative to data (3–10%). The tagging variables are then re-calculated. The N_{tags} distribution is recalculated with the new

values. The systematic uncertainty is assigned as the relative change in events, bin by bin in N_{tags}. For the two tag bin, this varies from 1 to 30% depending on the mass and lifetime. The mismodeling of α_{max} is found to have a negligible effect on the signal efficiency as the requirement is relatively loose.

The systematic uncertainty on the modeling of the online tracking efficiency is obtained by studying the online regional track reconstruction in data and MC. The online values of IP^{2D} and $IP^{\text{2D}}_{\text{sig}}$ are varied by the magnitude of the mismodeling found in events collected in control triggers. The new values are used to determine if the event would still pass at least one of the trigger paths and its associated offline H_{T} requirement. The N_{tags} distribution is recalculated with the values varied up and down. The relative change in the number of events per bin is taken as the systematic uncertainty. For the two tag bin, this uncertainty varies from 1 to 35%.

All signal systematic uncertainties are calculated individually for each model for all individual mass and lifetime points, and for each value of N_{tags} in the signal region.

5.8 Results and interpretation

The numerical values for the expected and observed yields are summarized in Table 5.9. The observed yields are found to be consistent with the predicted background, within the statistical and systematic uncertainties. No evidence for a signal at large values of N_{tags} is observed.

Exclusions for each model are obtained from the predicted and observed event yields in Table 5.9 and the signal efficiencies in Tables 5.3–5.4. All bounds are derived at 95% confidence-level (CL) according to the CL_s prescription [12, 13, 14] in the asymptotic approximation. For each limit derivation, we consider events with $N_{\text{tags}} \geq 2$ using independent bins for $N_{\text{tags}} = 2$ and $N_{\text{tags}} \geq 3$. Finer binning of the tag multiplicity for $N_{\text{tags}} > 3$ is found to have a negligible affect on the expected limits.

Cross section upper limits are presented as a function of the mass and lifetime of the parent particle. The analysis sensitivity is maximal for $(10 < c\tau_0 < 1000)$mm. Mass exclusion bounds at fixed lifetime are also derived, comparing the excluded cross section with the values predicted for the benchmark models described in section 5.5. In the case of SUSY models, the next-to-leading order (NLO) and next-to-leading-logs (NLL) $\tilde{t}\tilde{t}$ production cross section is used as reference, computed in the large-mass limit for all the other SUSY particles [15, 16, 17, 18, 19, 20].

Figures 5.4 and 5.5 show the excluded pair-production cross section for the Jet-Jet and Light-Light models, respectively. Cross sections as small as 1.2 fb are excluded for $c\tau_0 = 50$mm for both models. Exclusion limits are also derived for resonances decaying to $b\ell$ final states, as shown in Fig. 5.6. The sensitivity is similar to what is observed for the Jet-Jet model, although less stringent as additional jets give higher efficiency than additional leptons from both the tagging and triggering perspectives. Cross sections larger than 2.47 fb are excluded at 95% CL, for $c\tau_0$ in the range 70–100 mm excluding a parent mass value of 1135 GeV.

Figures 5.7 and 5.8 show the exclusions on the B-Tau and B-Ele models, respectively. The two models have similar performance at high mass with slightly stronger limits for the B-Ele model at lower mass $m_{\tilde{t}} = 300$ GeV and lifetimes $c\tau_0 > 10$mm. The highest mass excluded in the B-Ele (B-Tau) model occurs at $m_{\tilde{t}} = 1150$ (1155)GeV and $c\tau_0 = 70$ (70)mm at an observed cross section upper limit of 2.25 (2.17) fb at 95% CL.

In contrast, Fig. 5.9 shows the exclusion for the B-Mu model. Since the analysis uses jets reconstructed from calorimetric deposits while the two muons have small or no associated calorimeter deposit, the signal reconstruction efficiency and displaced-jet multiplicity are smaller in this case. This results in a weaker exclusion bound. The highest mass excluded in the B-Mu model occurs at $m_{\tilde{t}} = 1090$ GeV and $c\tau_0 = 70$mm at an observed cross section upper limit of 3.36 fb at 95% CL.

Table 5.2: Signal efficiency for fixed $m_X = m_{\tilde{t}} = 300$ GeV and varied $c\tau_0$ with modified branching ratios relative to the Jet-Jet and B-Lepton models. Selection requirements are cumulative from the first to the last row.

Light-Light				
m_X [GeV]	300	300	300	300
$c\tau_0$ [mm]	1	10	100	1000
≥ 2 tags	2.20 ± 0.19%	40.49 ± 0.80%	54.92 ± 0.93%	14.55 ± 0.47%
Trigger	2.04 ± 0.18%	39.16 ± 0.78%	39.63 ± 0.79%	8.20 ± 0.36%
Event sel.	2.03 ± 0.18%	38.41 ± 0.77%	36.99 ± 0.76%	6.89 ± 0.33%
≥ 3 tags	0.187 ± 0.054%	14.77 ± 0.48%	16.70 ± 0.51%	1.48 ± 0.15%
≥ 4 tags	–	5.11 ± 0.28%	4.73 ± 0.27%	0.216 ± 0.058%
B-Ele				
$m_{\tilde{t}}$ [GeV]	300	300	300	300
$c\tau_0$ [mm]	1	10	100	1000
≥ 2 tags	0.807 ± 0.093%	20.51 ± 0.47%	39.01 ± 0.65%	11.46 ± 0.35%
Trigger	0.398 ± 0.065%	14.68 ± 0.40%	22.95 ± 0.50%	5.15 ± 0.23%
Event sel.	0.398 ± 0.065%	13.92 ± 0.39%	20.34 ± 0.47%	3.58 ± 0.19%
≥ 3 tags	0.043 ± 0.022%	4.22 ± 0.21%	7.21 ± 0.28%	0.822 ± 0.093%
≥ 4 tags	–	0.727 ± 0.088%	1.19 ± 0.11%	0.053 ± 0.024%
B-Tau				
$m_{\tilde{t}}$ [GeV]	300	300	300	300
$c\tau_0$ [mm]	1	10	100	1000
≥ 2 tags	0.483 ± 0.073%	18.40 ± 0.45%	34.98 ± 0.61%	9.31 ± 0.32%
Trigger	0.439 ± 0.069%	14.63 ± 0.40%	20.20 ± 0.46%	3.81 ± 0.20%
Event sel.	0.406 ± 0.067%	12.45 ± 0.37%	15.50 ± 0.41%	2.37 ± 0.16%
≥ 3 tags	0.022 ± 0.016%	3.23 ± 0.19%	4.62 ± 0.22%	0.441 ± 0.069%
≥ 4 tags	–	0.525 ± 0.076%	0.660 ± 0.084%	0.022 ± 0.015%
B-Mu				
$m_{\tilde{t}}$ [GeV]	300	300	300	300
$c\tau_0$ [mm]	1	10	100	1000
≥ 2 tags	0.130 ± 0.037%	8.02 ± 0.29%	20.09 ± 0.46%	4.03 ± 0.21%
Trigger	0.054 ± 0.024%	3.97 ± 0.21%	6.63 ± 0.26%	0.881 ± 0.098%
Event sel.	0.043 ± 0.022%	2.92 ± 0.18%	4.21 ± 0.21%	0.489 ± 0.073%
≥ 3 tags	–	0.227 ± 0.049%	0.307 ± 0.057%	0.033 ± 0.019%
≥ 4 tags	–	0.011 ± 0.011%	–	–

Table 5.3: Signal efficiencies for the Jet-Jet and B-Lepton models with $c\tau_0 = 30$mm and varied mass. Selection requirements are cumulative from the first to the last row.

Jet-Jet

m_X [GeV]	50	100	300	1000
$c\tau_0$ [mm]	30	30	30	30
≥ 2 tags	2.710 ± 0.095%	14.80 ± 0.22%	54.24 ± 0.74%	79.93 ± 0.89%
Trigger	0.503 ± 0.041%	5.39 ± 0.13%	46.41 ± 0.68%	74.05 ± 0.86%
Event sel.	0.297 ± 0.031%	3.70 ± 0.11%	44.75 ± 0.67%	73.99 ± 0.86%
≥ 3 tags	0.050 ± 0.013%	1.087 ± 0.060%	20.87 ± 0.46%	49.42 ± 0.70%
≥ 4 tags	–	0.217 ± 0.027%	6.81 ± 0.26%	25.45 ± 0.50%

B-Lepton

$m_{\tilde{t}}$ [GeV]	300	600	800	1000
$c\tau_0$ [mm]	30	30	30	30
≥ 2 tags	31.52 ± 0.19%	47.32 ± 0.23%	52.53 ± 0.24%	55.88 ± 0.35%
Trigger	17.08 ± 0.14%	35.03 ± 0.20%	40.40 ± 0.21%	43.14 ± 0.30%
Event sel.	14.70 ± 0.13%	32.34 ± 0.19%	36.94 ± 0.20%	39.26 ± 0.29%
≥ 3 tags	4.106 ± 0.068%	10.76 ± 0.11%	13.29 ± 0.12%	15.00 ± 0.18%
≥ 4 tags	0.552 ± 0.025%	1.828 ± 0.045%	2.687 ± 0.055%	3.092 ± 0.082%

Table 5.4: Signal efficiency for fixed $c\tau_0$ = 30mm and varied mass with modified branching ratios relative to the Jet-Jet and B-Lepton models. Selection requirements are cumulative from the first to the last row.

Light-Light

m_X [GeV]	50	100	300	1000
$c\tau_0$ [mm]	30	30	30	30
≥ 2 tags	2.84 ± 0.12%	15.56 ± 0.29%	54.87 ± 0.92%	80.52 ± 1.11%
Trigger	0.530 ± 0.052%	5.70 ± 0.17%	47.14 ± 0.85%	74.85 ± 1.07%
Event sel.	0.327 ± 0.041%	3.90 ± 0.14%	45.68 ± 0.84%	74.80 ± 1.07%
≥ 3 tags	0.052 ± 0.016%	1.113 ± 0.076%	21.77 ± 0.58%	50.04 ± 0.88%
≥ 4 tags	–	0.230 ± 0.035%	7.38 ± 0.34%	25.80 ± 0.63%

B-Ele

$m_{\tilde{t}}$ [GeV]	300	600	800	1000
$c\tau_0$ [mm]	30	30	30	30
≥ 2 tags	39.01 ± 0.65%	53.70 ± 0.75%	59.62 ± 0.78%	62.42 ± 1.11%
Trigger	22.95 ± 0.50%	38.07 ± 0.63%	43.06 ± 0.66%	45.21 ± 0.95%
Event sel.	21.59 ± 0.48%	37.02 ± 0.62%	39.47 ± 0.64%	42.20 ± 0.92%
≥ 3 tags	7.86 ± 0.29%	14.28 ± 0.38%	17.37 ± 0.42%	20.39 ± 0.64%
≥ 4 tags	1.37 ± 0.12%	3.32 ± 0.19%	4.34 ± 0.21%	4.69 ± 0.31%

B-Tau

$m_{\tilde{t}}$ [GeV]	300	600	800	1000
$c\tau_0$ [mm]	30	30	30	30
≥ 2 tags	34.98 ± 0.61%	51.42 ± 0.73%	57.20 ± 0.76%	59.43 ± 1.07%
Trigger	20.20 ± 0.46%	39.78 ± 0.64%	45.46 ± 0.68%	47.62 ± 0.96%
Event sel.	17.17 ± 0.43%	37.47 ± 0.62%	43.64 ± 0.67%	44.26 ± 0.92%
≥ 3 tags	5.21 ± 0.24%	13.29 ± 0.37%	16.15 ± 0.40%	19.13 ± 0.61%
≥ 4 tags	0.86 ± 0.10%	3.09 ± 0.18%	3.68 ± 0.19%	4.48 ± 0.29%

B-Mu

$m_{\tilde{t}}$ [GeV]	300	600	800	1000
$c\tau_0$ [mm]	30	30	30	30
≥ 2 tags	20.09 ± 0.46%	35.46 ± 0.60%	41.18 ± 0.64%	43.13 ± 0.93%
Trigger	6.63 ± 0.26%	24.73 ± 0.50%	31.85 ± 0.56%	34.10 ± 0.82%
Event sel.	5.25 ± 0.24%	21.40 ± 0.47%	27.42 ± 0.52%	31.18 ± 0.79%
≥ 3 tags	0.344 ± 0.060%	3.03 ± 0.18%	5.28 ± 0.23%	6.08 ± 0.35%
≥ 4 tags	–	0.122 ± 0.035%	0.677 ± 0.082%	0.68 ± 0.12%

Table 5.5: The signal injection test using a fixed signal point $m_X = 700$ GeV and $c\tau_0 = 10mm$ with varied amount of injection. A summary of the 1,2,3, and 4 tag predictions as a function of the number of events injected (top). The two background systematic errors are listed separately as $\sigma_{method}, \sigma_{fake-rate}$. A summary of the observed number of tags (bottom).

Injection $\sigma \times \mathcal{L}$	**1 Tag Pred**	**2 Tag Pred**	**3 Tag Pred**	**4 Tag Pred**
0	$185^{+14,+17}_{-14,-13}$	$0.16^{+0.01,+0.03}_{-0.01,-0.02}$	$0.00^{+0.00,+0.00}_{-0.00,-0.00}$	$0.00^{+0.00,+0.00}_{-0.00,-0.00}$
10	$187^{+14,+17}_{-14,-13}$	$0.16^{+0.01,+0.03}_{-0.01,-0.02}$	$0.00^{+0.00,+0.00}_{-0.00,-0.00}$	$0.00^{+0.00,+0.00}_{-0.00,-0.00}$
100	$207^{+16,+18}_{-16,-14}$	$0.20^{+0.02,+0.04}_{-0.02,-0.03}$	$0.00^{+0.00,+0.00}_{-0.00,-0.00}$	$0.00^{+0.00,+0.00}_{-0.00,-0.00}$
1000	$408^{+31,+23}_{-31,-19}$	$0.81^{+0.06,+0.09}_{-0.06,-0.08}$	$0.00^{+0.00,+0.00}_{-0.00,-0.00}$	$0.00^{+0.00,+0.00}_{-0.00,-0.00}$
10000	$2366^{+177,+53}_{-177,-49}$	$26.95^{+2.02,+1.19}_{-2.02,-1.10}$	$0.18^{+0.01,+0.01}_{-0.01,-0.01}$	$0.00^{+0.00,+0.00}_{-0.00,-0.00}$
Injection $\sigma \times \mathcal{L}$	**1 Tag Obs**	**2 Tag Obs**	**3 Tag Obs**	**4 Tag Obs**
0	185.00	0.00	0.00	0.00
10	186.94	2.40	1.99	1.20
100	205.14	23.05	20.45	11.89
1000	386.10	237.20	188.40	116.80
10000	2260.00	2341.00	1976.00	1165.00

Table 5.6: Signal injection test with fixed number of injected events and varied $c\tau_0$ and m_X. A summary of the 1,2,3, and 4 tag predictions as a function of the number of events injected (top). The two background systematic errors are listed separately as $\sigma_{method}, \sigma_{fake-rate}$. A summary of the observed number of tags (bottom).

$\sigma \times \mathcal{L}$	**Mass** [GeV]	$c\tau_0$ [mm]	**1 Tag Pred**	**2 Tag Pred**	**3 Tag Pred**	**4 Tag Pred**
100	700	10	$207^{+16,+18}_{-16,-14}$	$0.20^{+0.02,+0.04}_{-0.02,-0.03}$	$0.00^{+0.00,+0.00}_{-0.00,-0.00}$	$0.00^{+0.00,+0.00}_{-0.00,-0.00}$
100	700	1000	$202^{+15,+18}_{-15,-14}$	$0.20^{+0.02,+0.03}_{-0.02,-0.03}$	$0.00^{+0.00,+0.00}_{-0.00,-0.00}$	$0.00^{+0.00,+0.00}_{-0.00,-0.00}$
1000	100	10	$222^{+17,+18}_{-17,-14}$	$0.23^{+0.02,+0.04}_{-0.02,-0.03}$	$0.00^{+0.00,+0.00}_{-0.00,-0.00}$	$0.00^{+0.00,+0.00}_{-0.00,-0.00}$
1000	100	1000	$195^{+15,+17}_{-15,-13}$	$0.18^{+0.01,+0.03}_{-0.01,-0.02}$	$0.00^{+0.00,+0.00}_{-0.00,-0.00}$	$0.00^{+0.00,+0.00}_{-0.00,-0.00}$
$\sigma \times \mathcal{L}$	**Mass** [GeV]	$c\tau_0$ [mm]	**1 Tag Obs**	**2 Tag Obs**	**3 Tag Obs**	**4 Tag Obs**
100	700	10	205.14	23.05	20.45	11.89
100	700	1000	211.56	17.98	9.04	3.62
1000	100	10	403.57	74.33	20.97	5.13
1000	100	1000	320.64	22.92	3.60	0.39

Table 5.7: A summary of the size of the signal injected in the signal injection test (top). A summary of signal region yields in the 2,3, and 4 nominal displaced jet tag bins (middle) and the observed number of tags (bottom), as a function of the size of the signal contamination, for a signal injection test using a fixed signal point $m_X = 700$ GeV and $c\tau_0 = 10$ mm with varied signal yields. The no signal case is included as a reference to the predicted values without contamination. The test is normalized such that the sum of signal and background events stays fixed at the observed number of events passing the analysis event selection. The contamination fraction corresponds to the hypothetical fraction of signal events contained within the events passing the event selection.

Contamination Fraction	**Signal σ [fb]**
0	0
0.01%	30
0.10%	290
1.04%	3000
9.47%	28000

Contamination Fraction	**2 tag prediction**	**3 tag prediction**	**4 tag prediction**
0	$1.34^{+0.25}_{-0.17}$	-	-
0.01%	$1.34^{+0.25}_{-0.17}$	-	-
0.10%	1.67 ± 0.33	-	-
1.04%	$6.71^{+0.91}_{-0.82}$	-	-
9.47%	205.38 ± 15.21	1.37 ± 0.08	-

Contamination Fraction	**2 tag observed**	**3 tag observed**	**4 tag observed**
0.00%	0	0	0
0.01%	19	16	10
0.10%	179	159	93
1.04%	1914	1520	943
9.47%	17632	14883	8775

Table 5.8: Summary of the systematic uncertainties. When the uncertainty depends on the specific features of the models (mass, lifetime and decay mode of the long-lived particle) a range is quoted, which refers to the computed uncertainty for $N_{\text{tags}} = 2$ events.

Signal systematic uncertainty	**Effect on yield**
H_{T} trigger inefficiency	5.0%
Jet p_t trigger inefficiency	5.0%
Trigger online tracking modeling	1.0–35.0%
Luminosity	2.7%
Acceptance due to PDF	1.0–6.0%
Displaced-jet tag variable modeling	1.0–30.0%

Table 5.9: The predicted and observed number of events as a function of N_{tags}. The prediction is based on the mistagging probability derived from events with fewer than two tags. The full event selection is applied. The quoted uncertainty corresponds to the total background systematic uncertainty.

$N_{\textbf{tags}}$	**Expected**	**Observed**
2	$1.09^{+0.16}_{-0.15}$	1
$\geq$ 3	$(4.9 \pm 1.0) \times 10^{-4}$	0

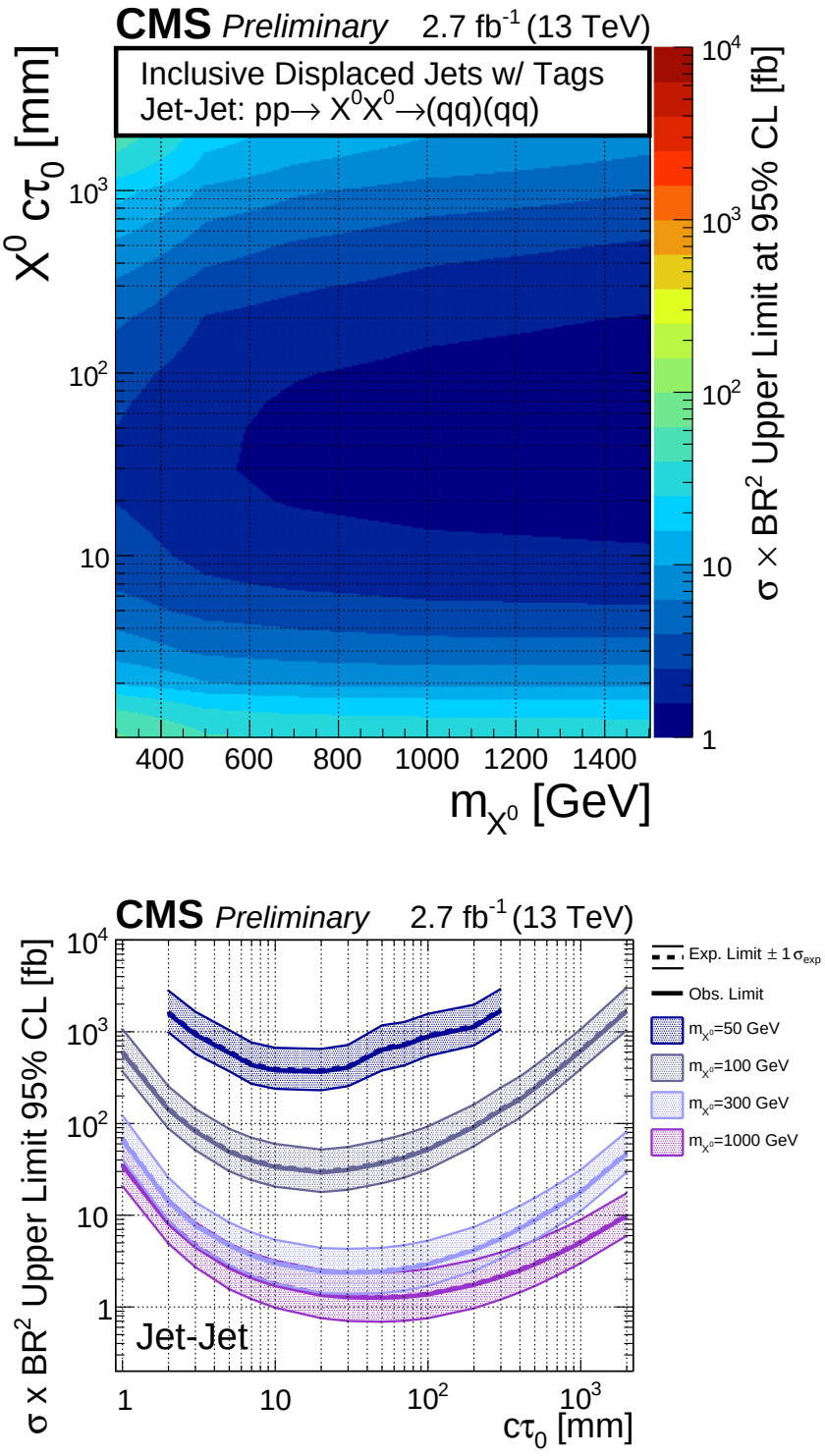

Figure 5.4: The excluded cross section at 95% CL for the Jet-Jet model as a function of the mass and lifetime of the parent particle X^0 (top) and as a function of the lifetime for four values of the mass (bottom).

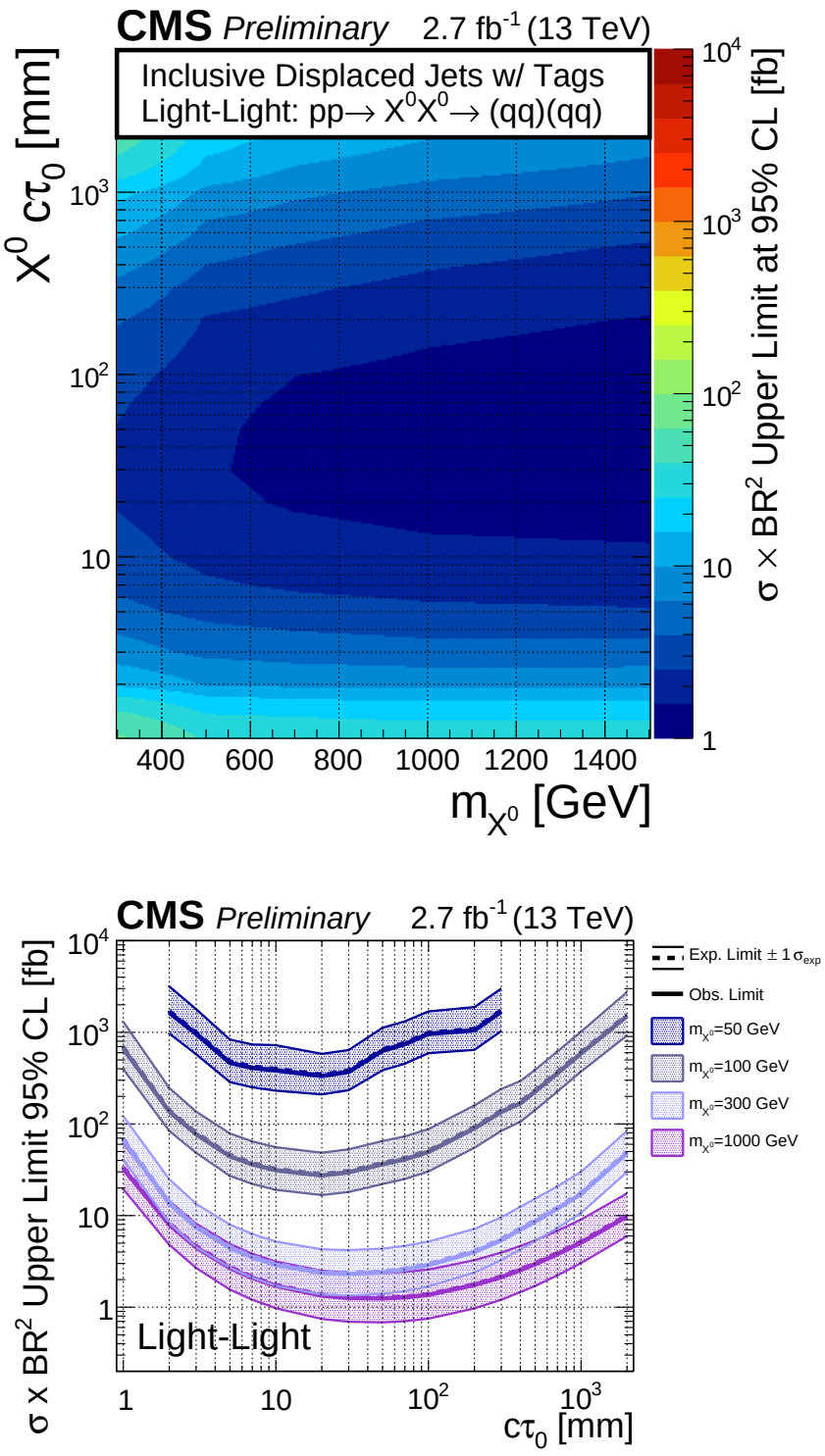

Figure 5.5: The excluded cross section at 95% CL for the Light-Light model as a function of the mass and lifetime of the parent particle X^0 (top) and as a function of the lifetime for four values of the mass (bottom).

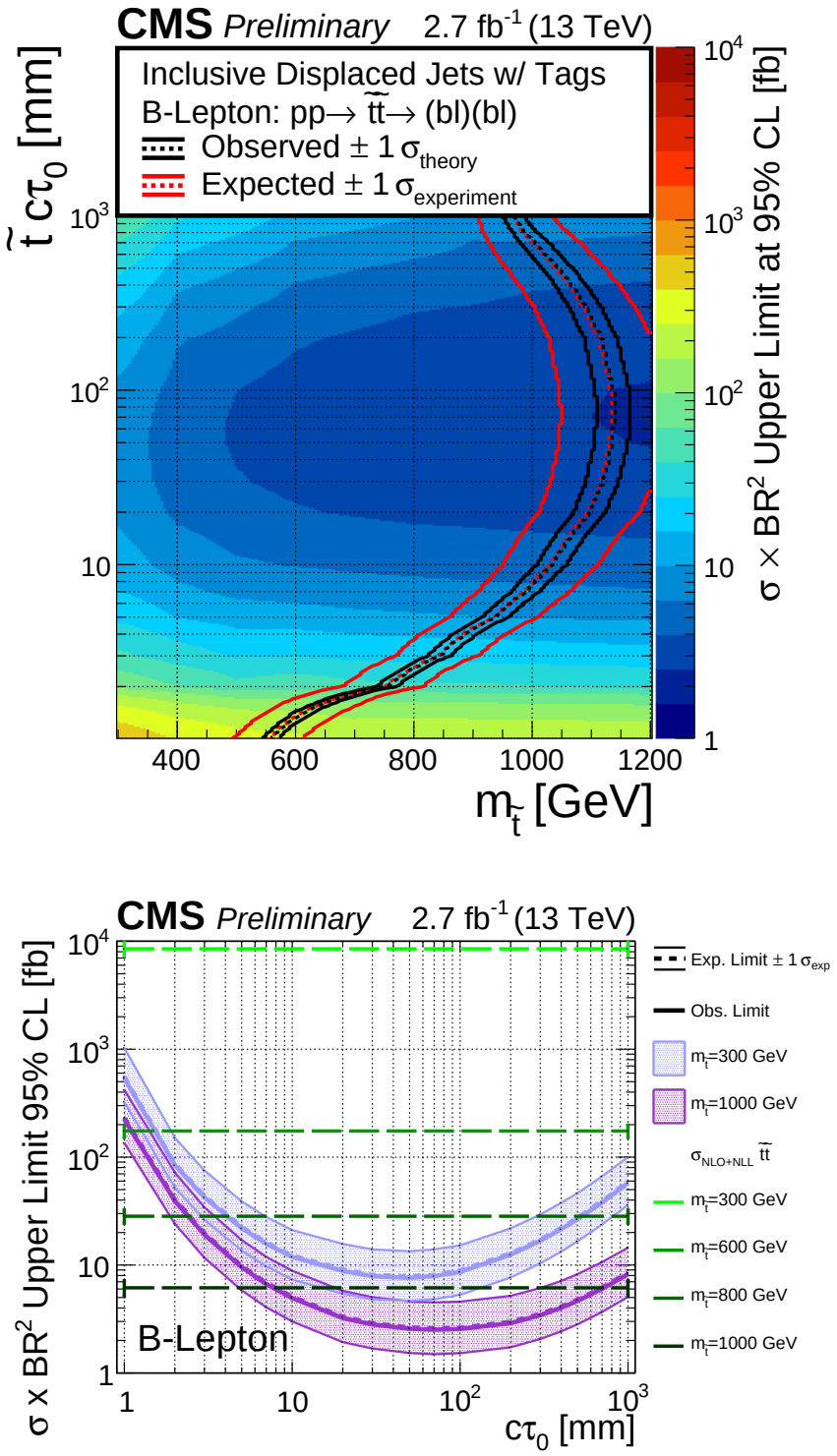

Figure 5.6: The excluded cross section at 95% CL for the B-Lepton model as a function of the mass and lifetime of the parent particle $\tilde{t}$ (top) and as a function of the lifetime for two values of the mass (bottom). The bottom plot also shows the expected upper limits with one standard deviation uncertainties.

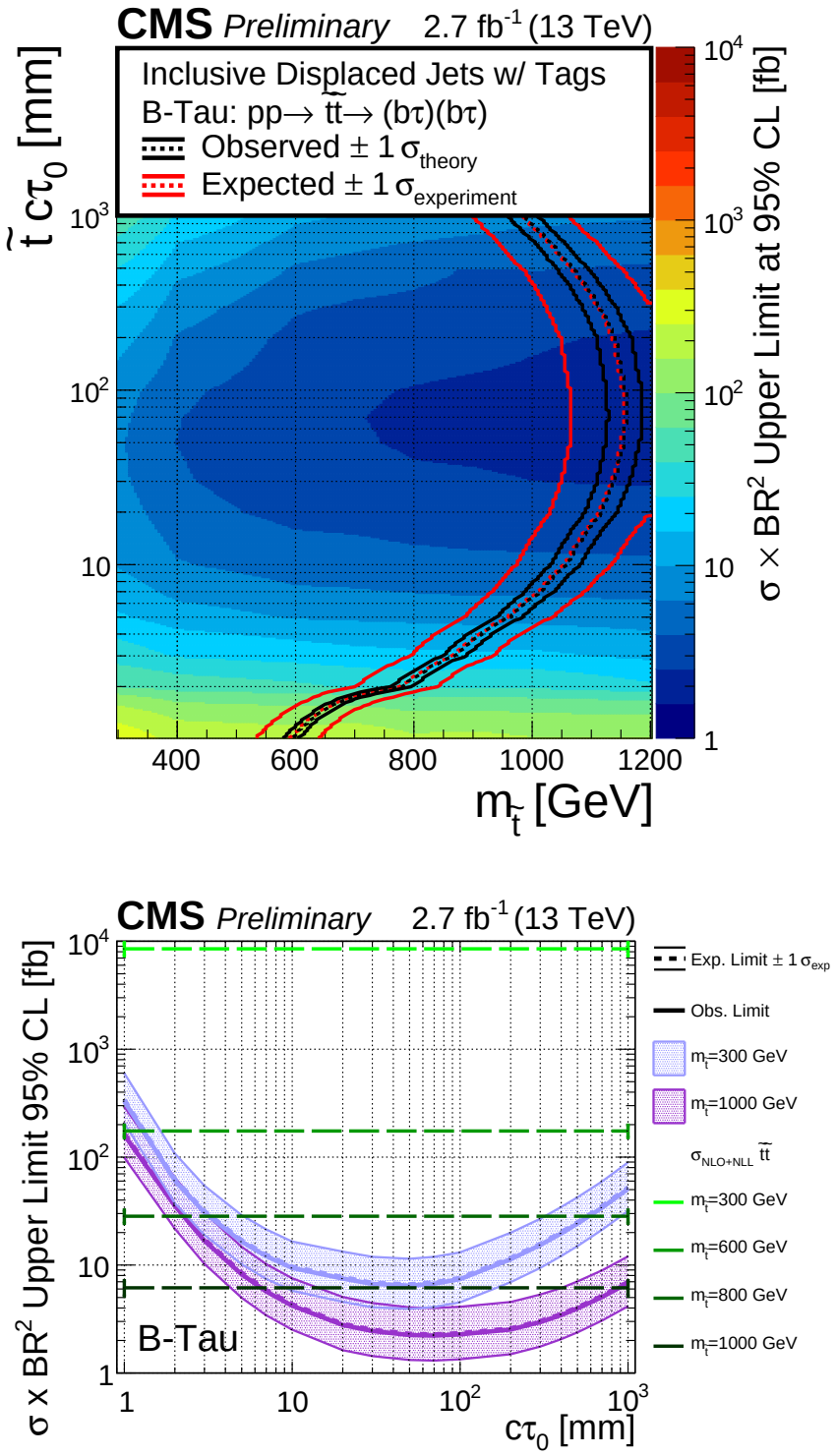

Figure 5.7: The excluded cross section at 95% CL for the B-Tau model as a function of the mass and lifetime of the parent particle $\tilde{t}$ (top) and as a function of the lifetime for two values of the mass (bottom). The bottom plot also shows the expected upper limits with one standard deviation uncertainties.

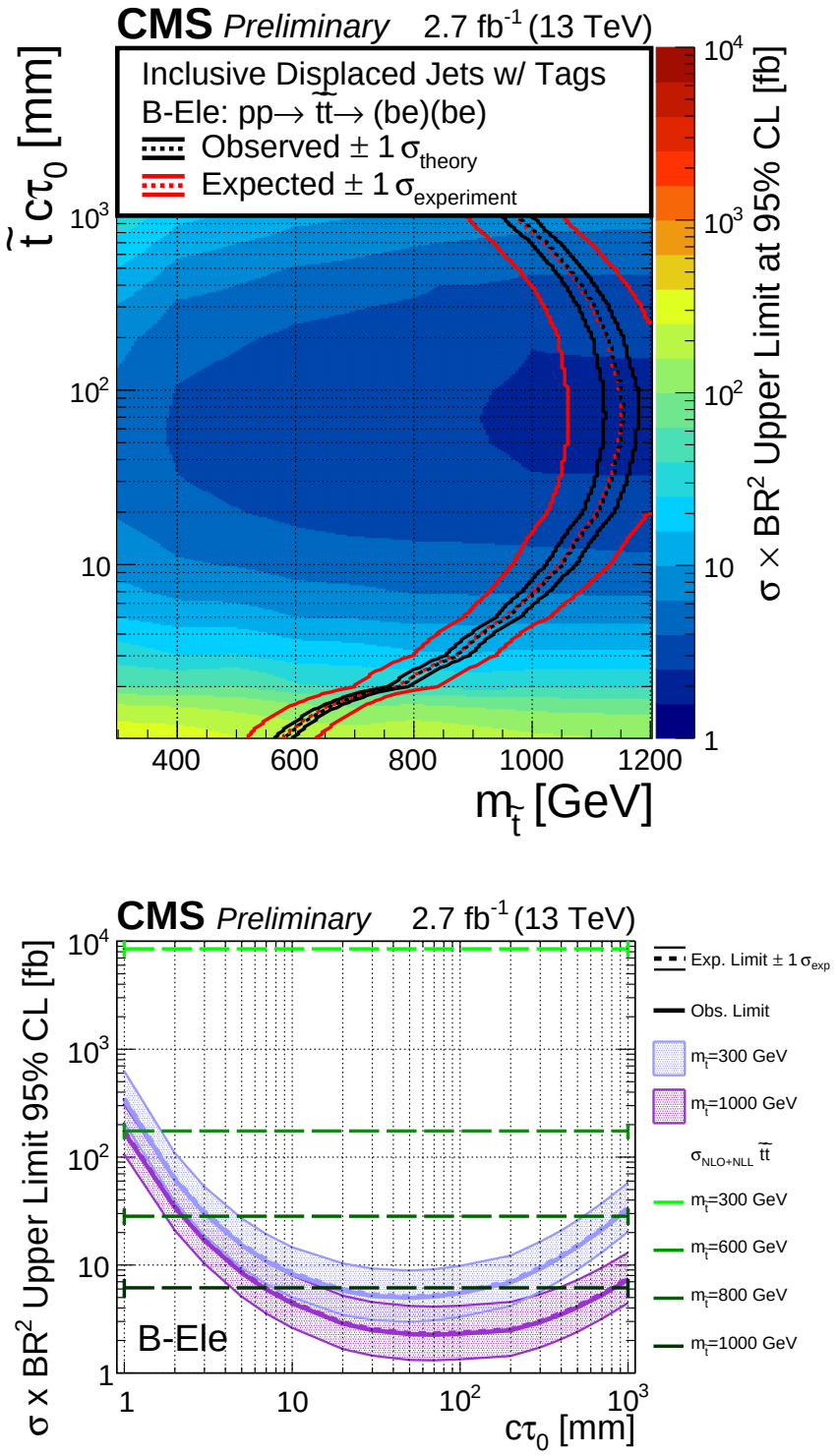

Figure 5.8: The excluded cross section at 95% CL for the B-Ele model as a function of the mass and lifetime of the parent particle $\tilde{t}$ (top) and as a function of the lifetime for four values of the mass (bottom). The bottom plot also shows the expected upper limits with one standard deviation uncertainties.

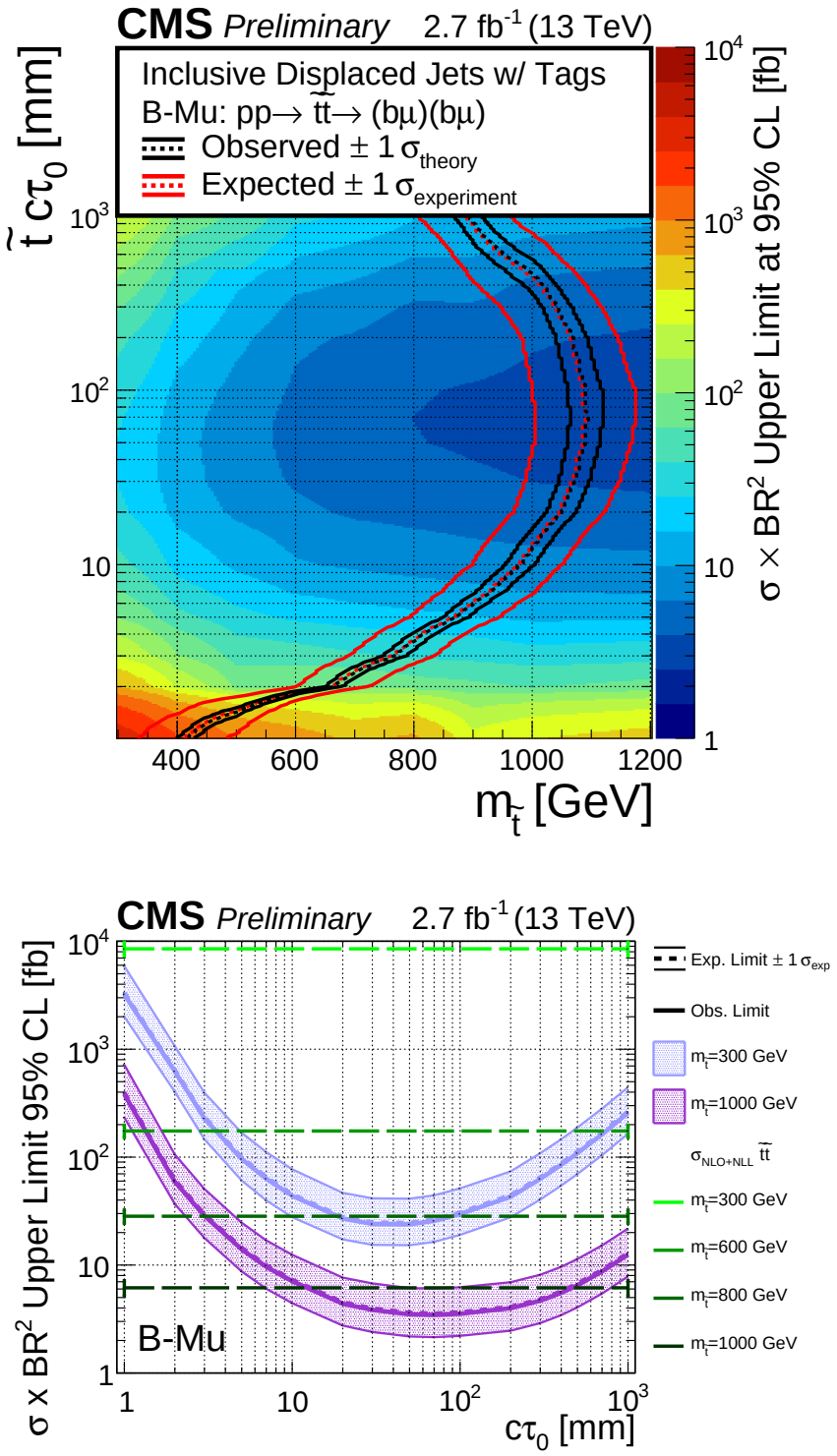

Figure 5.9: The excluded cross section at 95% CL for the B-Mu model as a function of the mass and lifetime of the parent particle $\tilde{t}$ (top) and as a function of the lifetime for four values of the mass (bottom). The bottom plot also shows the expected upper limits with one standard deviation uncertainties.

Bibliography

[1] J. Dalton. *A New System of Chemical Philosophy.* Manchester, 1808.

[2] Georges Aad et al. Search for long-lived, weakly interacting particles that decay to displaced hadronic jets in proton-proton collisions at $\sqrt{s} = 8$ TeV with the atlas detector. *Phys. Rev. D*, 92:012010, 2015.

[3] Georges Aad et al. Search for massive, long-lived particles using multitrack displaced vertices or displaced lepton pairs in pp collisions at $\sqrt{s} = 8$ TeV with the ATLAS detector. *Phys. Rev. D*, 92:072004, 2015.

[4] Vardan Khachatryan et al. Search for Long-Lived Neutral Particles Decaying to Quark-Antiquark Pairs in Proton-Proton Collisions at $\sqrt{s} = 8$ TeV. *Phys. Rev. D*, 91:012007, 2015.

[5] Matteo Cacciari, Gavin P. Salam, and Gregory Soyez. Fastjet user manual. *Eur. Phys. J. C*, 72, 2012.

[6] Matteo Cacciari, Gavin P. Salam, and Gregory Soyez. The anti-k_t jet clustering algorithm. *JHEP*, 04:063, 2008.

[7] T. Sjöstrand, Stephen Mrenna, and Peter Z. Skands. A brief introduction to PYTHIA 8.1. *Comput. Phys. Commun.*, 178:852, 2008.

[8] R. et al Ball. Parton distributions with LHC data. *Nucl. Phys. B*, 867:244, 2013.

[9] M. Strassler and Zurek K. Discoverying the higgs through highly displaced vertices. *Phys. Lett. B*, 263, 2008.

[10] P. Graham, D. Kaplan, S. Rajendran, and P. Sarawat. Displaced supersymmetry. *Journal of High Energy Physics*, 149, 2012.

[11] CMS Luminosity Measurement for the 2015 Data Taking Period. Technical Report CMS-PAS-LUM-15-001, CERN, Geneva, 2016.

[12] A. L. Read. Presentation of search results: the CL_s technique. *J. Phys. G*, 28:2693, 2002.

[13] Thomas Junk. Confidence level computation for combining searches with small statistics. *Nucl. Instrum. Meth. A*, 434:435, 1999.

[14] CMS and ATLAS Collaborations. Procedure for the lhc higgs boson search combination in summer 2011. CMS-NOTE-2011-005, 2011.

[15] W. Beenakker, R. Höpker, M. Spira, and P. M. Zerwas. Squark and gluino production at hadron colliders. *Nucl. Phys. B*, 492:51, 1997.

[16] A. Kulesza and L. Motyka. Threshold resummation for squark-antisquark and gluino-pair production at the LHC. *Phys. Rev. Lett.*, 102:111802, 2009.

[17] A. Kulesza and L. Motyka. Soft gluon resummation for the production of gluino-gluino and squark-antisquark pairs at the LHC. *Phys. Rev. D*, 80:095004, 2009.

[18] W. Beenakker, S. Brensing, M. Krämer, A. Kulesza, E. Laenen, and I. Niessen. Soft-gluon resummation for squark and gluino hadroproduction. *JHEP*, 12:041, 2009.

[19] W. Beenakker, S. Brensing, M. Krämer, A. Kulesza, E. Laenen, L. Motyka, and I. Niessen. Squark and gluino hadroproduction. *Int. J. Mod. Phys. A*, 26:2637, 2011.

[20] M. Krämer, A. Kulesza, R. van der Leeuw, M. Mangano, S. Padhi, T. Plehn, and X. Portell. Supersymmetry production cross sections in pp collisions at $\sqrt{s} = 7$ TeV. 2012.